Article

Neuron

PET Imaging of Tau Deposition in the Aging Human Brain

Highlights

- AV-1451 PET imaging allows in vivo Braak tau staging based on tracer uptake
- Age and β-amyloid are associated with different patterns of tau tracer retention
- Medial temporal tau tracer retention relates to episodic memory decline in aging

Authors

Michael Schöll, Samuel N. Lockhart, Daniel R. Schonhaut, ..., Henry D. Schwimmer, Gil D. Rabinovici, William J. Jagust

Correspondence

jagust@berkeley.edu

In Brief

Schöll, Lockhart, et al. examined tau pathology in vivo using ^{18}F-AV-1451 (tau) PET in healthy aging and found relationships with cognitive function. Confirming neuropathologically established patterns, they also detected different effects of age and β-amyloid on patterns of tau deposition.

Schöll et al., 2016, Neuron *89*, 971–982
March 2, 2016
http://dx.doi.org/10.1016/j.neuron.2016.01.028

CellPress

Neuron
Article

PET Imaging of Tau Deposition in the Aging Human Brain

Michael Schöll,[1,2,6] Samuel N. Lockhart,[1,6] Daniel R. Schonhaut,[3] James P. O'Neil,[4] Mustafa Janabi,[4] Rik Ossenkoppele,[1,3,5] Suzanne L. Baker,[4] Jacob W. Vogel,[1] Jamie Faria,[4] Henry D. Schwimmer,[1] Gil D. Rabinovici,[1,3,4] and William J. Jagust[1,4,*]

[1]Helen Wills Neuroscience Institute, University of California, Berkeley, Berkeley, CA 94720, USA
[2]MedTech West and the Department of Clinical Neuroscience and Rehabilitation, University of Gothenburg, 413 45 Gothenburg, Sweden
[3]Department of Neurology, Memory and Aging Center, University of California, San Francisco, San Francisco, CA 94158, USA
[4]Lawrence Berkeley National Laboratory, Berkeley, CA 94720, USA
[5]Department of Neurology & Alzheimer Center, Neuroscience Campus Amsterdam, VU University Medical Center, 1081 HV Amsterdam, the Netherlands
[6]Co-first author
*Correspondence: jagust@berkeley.edu
http://dx.doi.org/10.1016/j.neuron.2016.01.028

SUMMARY

Tau pathology is a hallmark of Alzheimer's disease (AD) but also occurs in normal cognitive aging. Using the tau PET agent ^{18}F-AV-1451, we examined retention patterns in cognitively normal older people in relation to young controls and AD patients. Age and β-amyloid (measured using PiB PET) were differentially associated with tau tracer retention in healthy aging. Older age was related to increased tracer retention in regions of the medial temporal lobe, which predicted worse episodic memory performance. PET detection of tau in other isocortical regions required the presence of cortical β-amyloid and was associated with decline in global cognition. Furthermore, patterns of tracer retention corresponded well with Braak staging of neurofibrillary tau pathology. The present study defined patterns of tau tracer retention in normal aging in relation to age, cognition, and β-amyloid deposition.

INTRODUCTION

Two pathological proteins that accumulate in the brains of Alzheimer's disease (AD) patients are β-amyloid (Aβ) as amyloid plaques, and hyperphosphorylated forms of the microtubule-associated protein tau assembling into neurofibrillary tangles (NFT). Neuropathological studies have repeatedly demonstrated that these aggregated proteins also accumulate in the brains of cognitively healthy older people (Bennett et al., 2006; Davis et al., 1999). The temporal and regional relations of these proteins to one another, to neurodegenerative processes, and to cognitive function have been studied for decades with post-mortem neuropathology (Braak and Braak, 1991; Braak et al., 2011; Price and Morris, 1999; Tomlinson et al., 1968). These studies often found normal aging to be associated with accumulation of tau pathology in the form of NFTs in the medial temporal lobe, particularly perirhinal and entorhinal cortex even in the absence of Aβ (Braak et al., 2011). This condition was recently termed primary age-related tauopathy (PART; Crary et al., 2014; Jellinger et al., 2015), although PART has also been suggested to be part of the AD spectrum (Duyckaerts et al., 2015). The spread of tau outside MTL is usually associated with the co-occurrence of amyloid plaques (Price and Morris, 1999; Tomlinson et al., 1968). Tau rather than Aβ pathology has also been shown to be closely related to cognition, predominantly memory decline, in post-mortem studies of both aging and AD (Arriagada et al., 1992; Ghoshal et al., 2002; Mitchell et al., 2002; Nelson et al., 2012; Rolstad et al., 2013; van Rossum et al., 2012).

In a landmark publication, Braak and Braak (Braak and Braak, 1991) meticulously analyzed 83 brains and staged AD-related pathology according to anatomical involvement patterns. Braak stages of tau pathology, derived from cross-sectional data, propose how AD-related tau pathology may begin in medial temporal structures, namely transentorhinal cortex, then extend to limbic areas of medial and inferior temporal lobe, to posterior cingulate cortex, and then widely into isocortical brain areas. These findings have been replicated (Braak et al., 2006; Braak et al., 2011; Serrano-Pozo et al., 2011), and eventually incorporated into AD neuropathological criteria (Hyman et al., 2012).

The interactions between age, Aβ, and tau accumulation have previously only been studied in post-mortem brain tissue, in vivo in animal models, or by using measures of total or hyperphosphorylated tau in cerebrospinal fluid (CSF). Existing data on tau distribution are based on neuropathological observations that represent a single endpoint in the disease process and have limitations compared to in vivo findings. Studies also frequently only sample selected brain regions and do not assess changes across the brain related to age, Aβ, or cognition (Braak et al., 2006, 2011; Braak and Braak, 1991; Serrano-Pozo et al., 2011). Conversely, CSF measures do not provide information on spatial accumulation patterns. The advent of positron emission tomography (PET) tau ligands enables, for the first time, tau pathology in living humans to be topographically mapped, quantified, and examined in relation to other aspects of cognitive aging.

Table 1. Demographics

	YA	OA	AD Patients
n	5	33	15
Age (years)	22.2 (2.3)[a,c]	78.6 (5.1)[b,c]	64.8 (9.2)[a,b]
Sex (M/F)	5/0	11/22	8/7
Education	15.0 (1.0)	16.3 (1.9)	16.5 (2.3) (2 N/A)
APOE (0/1/ 2 ε4 allele)	N/A	21 / 11 / 0 (1 N/A)	7 / 3 / 1 (4 N/A)
MMSE	29.3 (1.5)[c]	28.8 (1.2)	19.4 (5.2) (1 N/A)[a,b]
PiB+	N/A	16	14 (1 N/A)
Days between PiB and AV-1451 scans	N/A	105 (118)	62 (89) (1 N/A)
Days between NP and AV-1451 scan	43 (36) (1 N/A)	146 (101)	115 (90)
Days between NP and PiB scan	N/A	136 (95)	110 (94) (1 N/A)

All values are mean (SD) unless stated otherwise. *APOE*, Apolipoprotein E; DVR, distribution volume ratio; YA, young healthy adults; OA, old healthy adults; NP, neuropsychological examination.
[a]Significantly different (Mann-Whitney U test, $p < 0.05$) from OA patients.
[b]Significantly different (Mann-Whitney U test, $p < 0.05$) from YA patients.
[c]Significantly different (Mann-Whitney U test, $p < 0.05$) from AD patients.

^{18}F-AV-1451 (also known as ^{18}F-T807) is a PET ligand with high affinity for paired-helical filaments (PHFs), insoluble fibers composed of hyper-phosphorylated tau. Post-mortem tissue studies provided evidence that AV-1451 binds selectively to PHF tau but not Aβ or other common protein aggregates (Marquie et al., 2015; Xia et al., 2013). Human studies indicate binding patterns that parallel existing neuropathological staging of tau and that increase in the presence of cognitive impairment and dementia (Chien et al., 2013; Johnson et al., 2016).

Here, we examined in vivo the spatial extent of AV-1451 retention. One methodologic objective was to examine feasibility of replicating the Braak staging approach to describe in vivo tau accumulation patterns. Our overall goal was to explore relationships of the location of cortical tau ligand uptake with age, cognition, and Aβ deposition—as measured by the Aβ-binding ligand ^{11}C-PiB (Price et al., 2005)—in cognitively healthy older adults. Specifically, we hypothesized that AV-1451 uptake would be independently associated with age and PiB retention, would show negative relations to cognitive performance, and could enable subject-specific pathology staging.

RESULTS

Participants

We included five healthy young adults (YA, aged 20–26) and 33 cognitively healthy older adults (OA, aged 64–90) from the Berkeley Aging Cohort Study (BACS), and 15 patients with a diagnosis of probable AD dementia (McKhann et al., 2011; aged 53–77) from the University of California San Francisco (UCSF) Memory and Aging Center (MAC). The AD sample studied here (one participant diagnosed with behavioral/dysexecutive variant of AD, one with early-onset amnestic AD, three as late-onset amnestic AD, four with logopenic variant primary progressive aphasia, and six with posterior cortical atrophy) clinically does not represent a typical group of primarily late-onset amnestic AD. However, our goal in the current study was to provide data representative of high, clinical levels of tau pathology for the AV-1451 Braak staging procedure to be able to identify thresholds, and we thus included a variety of AD phenotypes in the AD participant sample.

Participant characteristics are provided in Table 1. Briefly, mean age differed significantly between all groups, while education levels were comparable. As expected, AD patients performed significantly worse on the Mini Mental State Examination (MMSE) than healthy participants.

Spatial Distribution of Tau

Figure 1 displays AV-1451 mean template space images for all groups. YA participants did not show observable cortical uptake. PiB-negative (PiB−) OA participants showed localized increases in temporal lobe regions, in particular medial temporal subregions (e.g., entorhinal cortex, parahippocampal gyrus), and in some OA participants in inferior and lateral temporal cortical regions. Uptake in PiB+ OA extended in most participants into inferior and lateral temporal lobe (particularly fusiform gyrus and inferior temporal cortex) and in some into lateral and medial parietal regions (including precuneus). Generally, elevated binding in OA was found in regions corresponding to Braak stages I–IV (see classification below). AD patients showed higher tracer retention in neocortical regions, particularly throughout temporal lobe, that also extended to encompass larger regions of parietal and frontal cortex. Primary sensory and motor regions rarely showed substantial tracer uptake, regardless of diagnostic status. All participants showed tracer retention in midbrain; OA and AD participants also showed retention in basal ganglia and a region dorsal to the hippocampus corresponding to choroid plexus. Uptake in these regions is thought to represent "off-target" binding of AV-1451 to targets other than tau (Marquie et al., 2015; see Discussion for details).

AV-1451 Uptake in Braak ROIs and In Vivo Braak Staging

In an attempt to reproduce traditional Braak staging of tau pathology based on neuropathological findings (Braak and Braak, 1991), we used weighted bilateral composite FreeSurfer-derived regions of interests (ROIs) approximating the anatomical definitions of transentorhinal (Braak stage I/II), limbic (III/IV), and isocortical (V/VI) Braak stages (Table S1, Movies S1, S2, and S3). In a first step, we examined AV-1451 retention within each group of ROIs uncorrected for partial volume effect and found, as expected, substantial differences between all three diagnostic groups (Figure 2A). Young adults had low uptake throughout all Braak ROIs, while OA showed overall higher values and more within-group variance. AD patients showed as expected the highest values and greatest within-group variance. Group differences were greatest ($p < 0.001$) between AD patients and OA for all Braak ROIs and between YA and OA in "early" Braak stage ROIs I/II and III/IV. Results were similar after partial volume effect correction (PVC) using the Geometric Transfer Matrix approach (Rousset et al., 1998; Figure 2B). PVC produced only a small

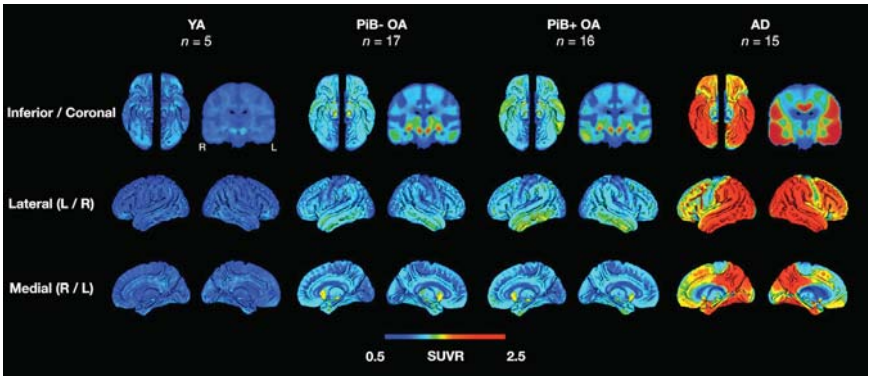

Figure 1. AV-1451 Mean Images of Participant Groups

Surface projections and coronal slices are presented for young healthy adults (YA), older adults (OA) split into PiB− and PiB+ subgroups for illustration, and AD patients. Differences between cognitively healthy participants were primarily localized in inferior and lateral temporal subregions, while patient versus control differences extended into other temporal as well as parietal and frontal cortical regions.

increase in the measurement of tracer retention in hippocampus, but a large increase in choroid plexus signal adjacent to the hippocampus, suggesting that choroid plexus PVC modeling may aid in the estimation of actual AV-1451 signal in adjacent regions such as hippocampus (Figure S1). For this reason, and because PV-corrected data distinguished OA marginally better from AD patients (Table S2), we used PV-corrected data in further native space ROI analyses.

Next, we calculated thresholds to assign a Braak stage to each participant based on Braak ROI AV-1451 uptake. We employed a conditional inference tree approach that embeds decision tree-structured regression models (Figure S2). In a first step, we entered the whole dataset into the model classifying all participants based on Braak V/VI ROI uptake. We found 13 out of 15 AD patients above the threshold suggested by the regression model (>2.79 mean SUVR); they were assigned Braak stage V/VI. The remaining participants underwent the same procedure, now using Braak III/IV ROI data. Two AD and six OA participants were classified as Braak III/IV (>1.725). Finally, using Braak I/II ROI data, 25 OA were classified as Braak I/II (>1.395), leaving 2 OA and the 5 YA in Braak stage 0. Figure 3 displays mean AV-1451 images for the participants in different Braak stages. These demonstrate clear progression of AV-1451 retention to inferior and lateral temporal lobe followed by further progression to other isocortical regions in final Braak stages. Characterizing participants according to their assigned Braak stage showed that with increasing stage there was also increasing global PiB distribution volume ratio (DVR) index (and proportion of PiB+ OA in each group; note only OA and AD participants had PiB measurements), increasing proportion of *APOE* ε4 allele carriers, declining MMSE scores, and declining hippocampal volumes (with the exception of AD patients in stage V/VI; hippocampal volume derived from FreeSurfer 5.1 parcellation, see Experimental Procedures). In healthy OA and YA, lower hippocampal volume showed a statistically significant relationship with higher Braak stage (Spearman's rho −0.45, p = 0.005); *APOE* status and PiB index exhibited too many missing values for meaningful statistical analysis.

AV-1451 and Cognition in Cognitively Healthy Elderly

We explored relations of cross-sectional (closest to AV-1451 scan) and retrospective longitudinal cognition with AV-1451 Braak ROI uptake in healthy elderly using regression models covarying for age and sex. Longitudinal cognitive data were available for 30 OA, followed on average for 4.1 ± 2.2 years prior to AV-1451 PET (4.0 ± 2.1 test sessions). Cognitive performance was evaluated using factor scores for episodic memory, working memory, processing speed, and an average of these domains as a measure for global cognition.

For episodic memory, increased Braak I/II ROI tracer binding predicted worse cross-sectional performance ($\beta = -3.12$, $p = 0.007$) and retrospective longitudinal decline (slopes; $\beta = -0.06$, $p = 0.006$; Figure 4A). Retrospective longitudinal impairment in global cognition was related to higher AV-1451 uptake in all Braak ROIs (I/II: $\beta = -0.013$, $p = 0.009$; III/IV: $\beta = -0.015$, $p < 0.001$; V/VI: $\beta = -0.07$, $p = 0.007$; Figure 4B). Scores for cross-sectional global cognition, cross-sectional or longitudinal working memory, and processing speed did not show any statistically significant relationship with AV-1451. A global mean AV-1451 retention measure (average of all Braak ROIs) was also generated and found only to be correlated with retrospective longitudinal change in global cognition. Crucially, this global retention measure was not correlated with either cross-sectional or longitudinal change in episodic memory ($p = 0.7$); only retention in Braak I/II ROIs was (as shown in Figure 4). This global mean measure was furthermore only marginally correlated with cortical PiB DVR ($p = 0.08$). We interpret these results as evidence that the regional characterization of tracer retention using our Braak ROI approach captures more information than does a global measure of AV-1451 retention.

To explore whether Aβ pathology influenced the effect of tau pathology on cognition, we added continuous cortical PiB DVR data to the statistically significant regression models and examined whether the p value for the association between AV-1451 and cognition changed after adjusting for PiB. All models remained significant except for the effect of Braak V/VI ROI AV-1451 on longitudinal change in global cognition, which disappeared when PiB was added the model. We did not observe statistically significant interactions between PiB and AV-1451, likely due to the small sample size. For the same reason, we refrained from performing mediation or moderation analyses to further explain directionalities.

We also explored direct relations between Aβ and cognition (Figure S3). Global PiB uptake was significantly associated with longitudinal global cognition change ($\beta = -0.09$, $p = 0.002$). When AV-1451 was added to the model, the effect survived

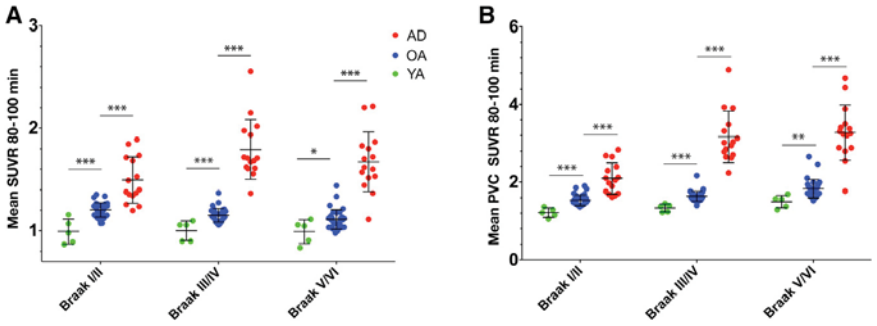

Figure 2. Braak Stage ROI AV-1451 Uptake by Group

(A) Results from Mann-Whitney U test, uncorrected for partial volume effects.

(B) Results from Mann-Whitney U test, corrected for partial volume effects. Lines indicate means ± SD. *p < 0.05, **p < 0.01, ***p < 0.001. See also Tables S1 and S2, Figure S1, and Movies S1, S2, and S3.

only for the model including Braak ROI I/II AV-1451 data, not for models including Braak ROI III/IV or V/VI data.

To confirm and explore the spatial relationship of AV-1451 binding with episodic memory, we conducted voxelwise nonparametric regressions of both cross-sectional episodic memory scores and longitudinal episodic memory slopes against whole-brain AV-1451 data. We found significant associations between higher AV-1451 and both worse episodic memory scores and greater decline; these clusters were localized to medial temporal lobe regions including parts of entorhinal cortex, parahippocampal gyrus, and hippocampus (Figure 5). Peak voxel MNI coordinates are reported in Table S3.

Voxelwise Associations between Age, PiB, and AV-1451 Accumulation among Cognitively Healthy Elderly

We used voxelwise nonparametric statistical tests to examine associations between age, PiB DVR (global cortical ROI), and AV-1451 accumulation. Statistical tests employed two thresholds, one liberal ($p < 0.005$ uncorrected height and $k \geq 100$ voxel cluster extent threshold) and one conservative ($p < 0.05$ family-wise error-corrected [FWE] height threshold); by design, conservative threshold results are not a subset of liberal results (see Experimental Procedures). We found positive associations of age with cortical AV-1451 accumulation (Figure 6A) and of PiB with cortical AV-1451 accumulation (Figure 6B). The relationships were independent of one another and spatially distinct. Negative associations of age or PiB with AV-1451 were not significant. Specifically, advancing age predicted AV-1451 accumulation in MTL (entorhinal cortex, hippocampus, and parahippocampal gyrus) and in ventral frontal cortex (basal forebrain) and insula. Increasing Aβ burden, however, predicted increased AV-1451 in regions beyond medial temporal lobe, particularly inferior and lateral temporal cortical regions, and medial and lateral parietal and frontal cortex. The results found using a combined uncorrected cluster and height threshold and with family-wise error correction were spatially overlapping. Voxelwise results were similar when controlling for sex, education, and gray matter volume as a proxy for cortical atrophy (data not shown). MNI coordinates of significant voxels for each association are reported in Table S4.

ROI Analyses

Examination of regional relations between age, PiB, and AV-1451 in temporal lobe subregions revealed spatially distinct associations consistent with voxelwise findings; age and PiB exhibited dissociable effects on AV-1451, with a medial-lateral dissociation of effects of age and global PiB on temporal AV-1451 (Figure 7). Significant associations between advancing age and greater AV-1451 accumulation were only present in entorhinal cortex and parahippocampal gyrus and were diminished in strength in more lateral regions. Conversely, associations between increasing global cortical PiB DVR and greater temporal AV-1451 accumulation were marginally significant in entorhinal cortex and increased in significance from parahippocampal gyrus to fusiform gyrus and inferior temporal cortex. Thus, from medial to inferolateral temporal cortex, there existed inverse relationships between age and AV-1451 and PiB and AV-1451.

DISCUSSION

In this study of cognitively healthy elderly people, we explored uptake patterns of ^{18}F-AV-1451, an in vivo PET biomarker for accumulation of PHF tau, and examined the relationships of regional and voxelwise tau accumulation with multiple factors. We consistently observed that tau accumulation occurred in anatomically specific patterns, in contrast to the more diffuse nature of Aβ deposition as measured with PiB PET. We also demonstrated the ability to segregate participants based on AV-1451 accumulation in specific Braak stages using a computational method. Furthermore, we found that AV-1451 was related to cross-sectional and longitudinal cognitive measures and that there were differences in the patterns associated with age and Aβ. Our results suggest that tau deposition, especially in MTL, is an important aspect of cognitive aging that may have behavioral consequences. They also suggest a relationship between tau and Aβ with implications for AD pathogenesis.

AV-1451 Uptake Patterns Are Present in the Healthy Aging Brain and Enable In Vivo Braak Staging of Tau Progression

The patterns of AV-1451 retention parallel findings in neuropathological studies (Braak and Braak, 1991, 1997; Serrano-Pozo et al., 2011), as well as a recent report indicating that the visual appearance of AV-1451 retention parallels Braak staging (Johnson et al., 2016). Although regions sampled for Braak staging may vary across neuropathology laboratories, our approach followed the NIA-AA recommendations (Hyman et al., 2012) and approximated the original and revised Braak stage definitions (Braak and Braak, 1991; Braak et al., 2006). Furthermore, the component regions that comprised these larger Braak ROIs

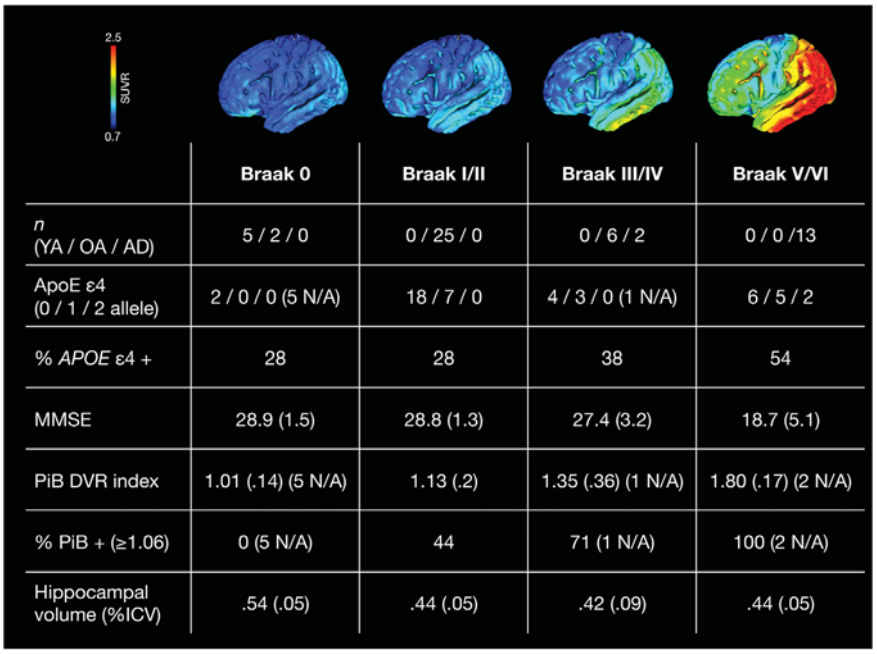

	Braak 0	Braak I/II	Braak III/IV	Braak V/VI
n (YA / OA / AD)	5 / 2 / 0	0 / 25 / 0	0 / 6 / 2	0 / 0 /13
ApoE ε4 (0 / 1 / 2 allele)	2 / 0 / 0 (5 N/A)	18 / 7 / 0	4 / 3 / 0 (1 N/A)	6 / 5 / 2
% *APOE* ε4 +	28	28	38	54
MMSE	28.9 (1.5)	28.8 (1.3)	27.4 (3.2)	18.7 (5.1)
PiB DVR index	1.01 (.14) (5 N/A)	1.13 (.2)	1.35 (.36) (1 N/A)	1.80 (.17) (2 N/A)
% PiB + (≥1.06)	0 (5 N/A)	44	71 (1 N/A)	100 (2 N/A)
Hippocampal volume (%ICV)	.54 (.05)	.44 (.05)	.42 (.09)	.44 (.05)

Figure 3. In Vivo Braak Staging Using Conditional Inference Trees

Braak staging of healthy young adults (YA, n = 5), healthy older adults (OA, n = 33) and AD patients (n = 15) based on AV-1451 Braak ROI uptake, with participant characterization by in vivo assigned Braak stage. ICV, intracranial volume. Values for MMSE, PiB DVR index, and hippocampal volume are mean (SD).

followed a predictable pattern in relation to cognition and amyloid (Figure 7).

Young adults showed minimal brain uptake, even in subcortical structures, consistent with Braak stage 0. The conditional inference tree analysis consistently assigned them to Braak 0 based on low AV-1451 uptake. Although there is evidence of tau accumulation in the young adult brainstem (Braak et al., 2011), PET resolution is likely inadequate to detect this. Older adults clearly showed tracer retention in medial temporal structures, with PIB+ individuals appearing to demonstrate more tau deposition in inferior and lateral temporal neocortex. These visual patterns were confirmed with Braak staging. Using our classification approach, most OA were classified as Braak stage I/II (76%), and a smaller proportion as Braak III/IV (18%) or stage 0 (6%); no healthy participants were classified as Braak stage V/VI. These numbers are congruent with neuropathological findings; Braak and Braak (Braak and Braak, 1997) reported 6% of all participants aged 70–80 years (n = 605) in Braak stage 0, 64% in Braak stage I/II, 25% in Braak stage III/IV, and 5% in Braak stage V/VI. While these proportions do not reference cognitive status, Bennett and colleagues (Bennett et al., 2006) examined 134 cognitively normal elderly (mean age at death 83 years) and found 2% in Braak 0, 38% in Braak I/II, 56% in Braak III/IV, and 4% in Braak V/VI. Although it is difficult to compare PET imaging with neuropathology, these results are in agreement with few normal older individuals in stages 0 and V/VI and most distributed between I/II and III/IV.

Differences between AD and healthy OA participants were more substantial. AD participants showed elevated tracer retention in early and middle Braak stage regions, and AD uptake patterns frequently encompassed larger regions of medial and lateral parietal and, to a lesser extent, frontal lobes. This was consistent with Braak stage V/VI, which was confirmed by our in vivo Braak staging, assigning 13 AD patients to Braak stage V/VI and two to III/IV.

These results have limitations. Our threshold-calculation approach was data driven and requires replication using separate cohorts to establish and validate threshold values that will likely differ. Nevertheless, these results provide proof-of-concept that in vivo Braak staging using tau PET is possible in cognitively healthy elderly. Further, by characterizing participants according to Braak stage, we also found, consistent with previous findings (Braak and Braak, 1991, 1997; Braak et al., 2006, 2011; Nelson et al., 2012; Serrano-Pozo et al., 2011), increasing Braak stage in cognitively healthy and diseased participants to be associated with increasing global amyloid burden, increasing *APOE* ε4 allele positivity, declining cognition, and reduced hippocampal volumes. The AD patients pose an exception to the relationship between tau and hippocampal volumes, perhaps because our AD group included many patients with early age of onset (mean age at PET 65) and non-amnestic clinical presentations, both of which are associated with neocortical-predominant neurodegeneration and relative sparing of MTL in terms of both atrophy and tau burden (Murray et al., 2011; Ossenkoppele et al., 2015a). In addition, age-related hippocampal atrophy in our older control group (on average 14 years older at PET than the AD group), may have decreased our ability to detect a relationship between AV-1451-defined Braak stage and hippocampal volumes in this sample.

Ultimately, given the current approach, we cannot say that participants characterized as Braak I/II are different from participants characterized as Braak 0 only in the Braak stage I/II ROIs. This is true for all the Braak stages in our approach: those in higher stages may in fact have more generalized AV-1451 deposition than those in lower stages. Our goal was not to strictly duplicate neuropathological classification, since imaging has both advantages and disadvantages compared with neuropathology. The obvious disadvantage is the poorer resolution of imaging, although the advantage is a whole-brain view of the distribution of tau pathology. However, Figure 3 in particular makes it clear that the classification of participants according to the 4 stages routinely used in neuropathology does indeed capture distributions that reflect medial temporal, limbic, and neocortical stages and that relate to a progression along a spectrum from youth through aging to dementia.

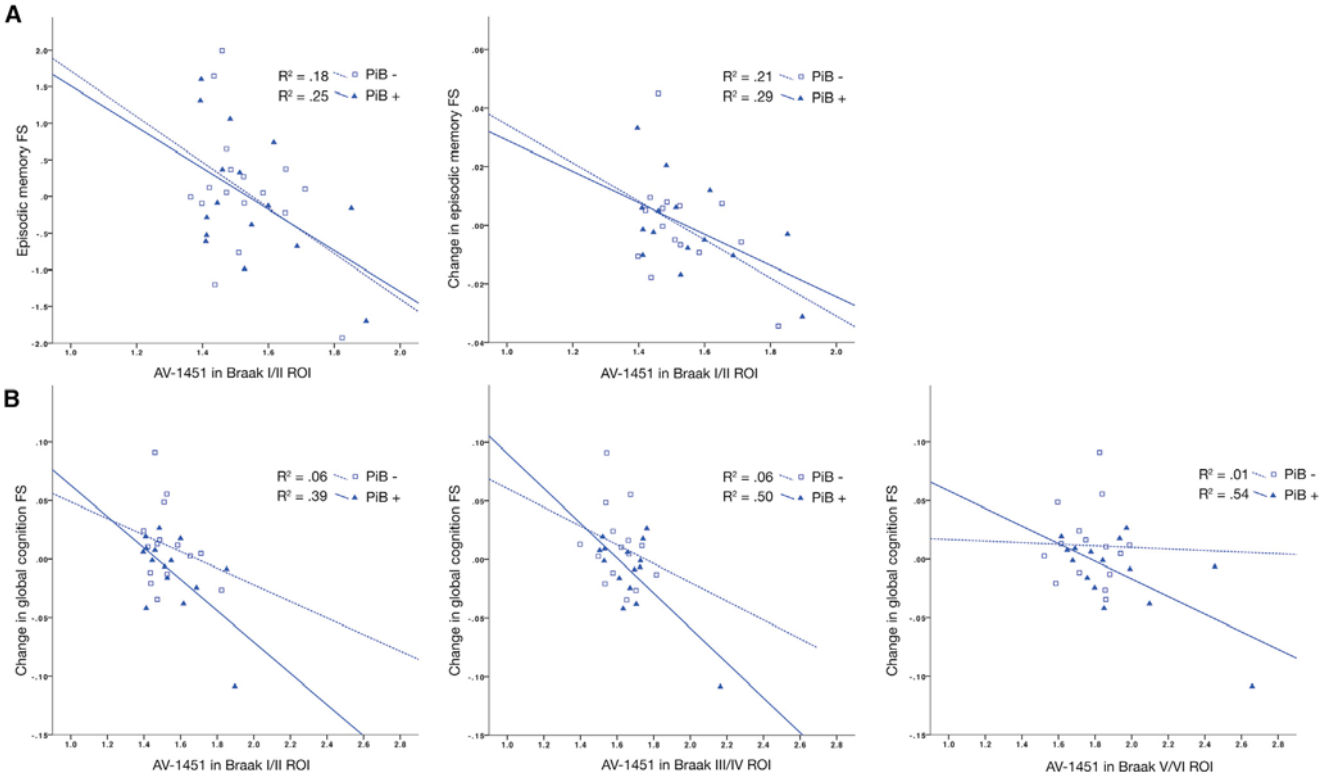

Figure 4. AV-1451 in Braak ROIs versus Cognition in Healthy Elderly

(A and B) Significant relationships of AV-1451 in Braak ROI I/II with cross-sectional performance and retrospective change (slopes) in episodic memory (A) and of AV-1451 in all Braak stage ROIs with retrospective change (slopes) in global cognition in healthy OA participants (B), grouped into PiB+ and PiB−. See also Figure S3.

Future attempts to replicate and extend this approach will require more diverse and "intermediate" participants (e.g., middle-aged healthy individuals, patients with mild cognitive impairment). It will be useful to investigate AV-1451 uptake using a multivariate approach, to independently derive uptake patterns and examine relations with Braak pathological staging; however, we do not yet have enough participants to address this. Even though this Braak ROI approach is tentative and despite its limitations, the fact that the ROI-based and voxelwise approaches showed similar relations with cognition and amyloid supports the application of the Braak ROI staging. ROI-based analyses furthermore allowed the use of PV-corrected data within native space. This permits more specific measurements of tracer uptake and direct testing of hypotheses, in contrast to more exploratory voxelwise methods.

Finally, the presumed off-target binding of this PET tracer in brainstem, basal ganglia, and choroid plexus may pose quantitation problems. The reason for this binding is unclear; while binding to MAO-A has been suggested, the results do not appear to reflect the quantity and distribution of this enzyme in the brain (Tong et al., 2013). Basal ganglia and midbrain binding are not likely to interfere with cortical measurement. While choroid plexus uptake complicates quantification in the hippocampus, we were able to ameliorate this problem through partial volume correction. Recent research has also suggested that neuromelanin or blood products may also contribute to AV-1451 signal (Marquie et al., 2015).

Tau Is Differentially Associated with Age and Amyloid Accumulation in OA

Tau pathology is near-universally present in aging (Bouras et al., 1994; Braak et al., 2011) and, based on cross-sectional pathological studies, may appear first in temporal lobe allocortex, specifically MTL, remaining mostly confined to these regions with moderate spread into neocortical temporal lobe and minor spread into other neocortical areas with age (Braak and Braak, 1991; Braak et al., 1996; Guillozet et al., 2003; Price and Morris, 1999; Serrano-Pozo et al., 2011). In CSF, elevated levels of tau, not altered levels of $A\beta_{42}$, are also strongly related with older age in normal people (Sjögren et al., 2001). Some pathologists have suggested that this may represent PART (Crary et al., 2014; Jellinger et al., 2015). In this model, accumulation of tau pathology occurs steadily throughout life, often restricted to MTL subregions such as entorhinal cortex and hippocampus, with little presence of additional neuropathology besides medial temporal atrophy (in the absence of substantial Aβ accumulation). The current findings of age-related increases in MTL tracer binding are in concordance with the initial concept of PART, including the relationship of hippocampal atrophy and MTL tau and the relative lack of Aβ deposition in individuals with tau confined to MTL. However, the current findings do not definitively support the idea that PART exists outside the AD continuum (Duyckaerts et al., 2015), nor can we be certain that there is a complete lack of neocortical tracer retention in Aβ-negative individuals.

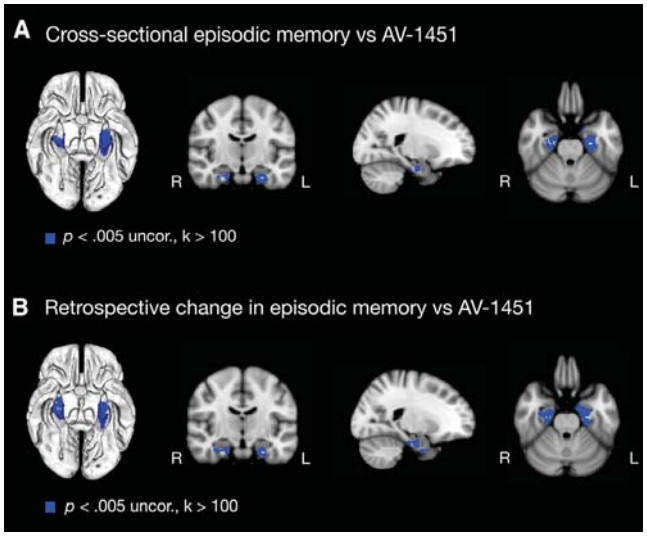

Figure 5. Cross-sectional and Longitudinal Episodic Memory versus AV-1451 Uptake in OA

(A and B) Nonparametric voxelwise regression of AV-1451 on cross-sectional performance (A) and retrospective longitudinal change (B) in episodic memory. See also Table S3.

The spread of tau outside MTL has been associated with increased Aβ pathology (Braak et al., 2006; Braak and Braak, 1991), and models of biomarker change in AD suggest that Aβ aggregation may play a facilitating role in the disease pathological cascade (Jack et al., 2013). Conversely, tau is consistently found in MTL regions before and in the absence of Aβ pathology (Crary et al., 2014; Fornicola et al., 2014; Price and Morris, 1999). Among OA, we found that while advancing age predicted greater tau accumulation in MTL and to some extent in ventral frontal cortex (a region also known to show early tau accumulation; Crary et al., 2014), increasing Aβ burden predicted tau spread outside medial temporal subregions into lateral and inferior temporal as well as other neocortical regions (Figure 6).

Our results support a model suggesting two diverging pathways for tau pathology in aging: one proposing MTL tau pathology as an effect of chronological age, another relating cortical tau pathology to interactions with cortical Aβ pathology (Price and Morris, 1999; Small and Duff, 2008). Studies in cell and transgenic mouse models suggest that tau in its harmful hyperphosphorylated form spreads from entorhinal cortex, likely in a *trans*-synaptic manner, along functional networks and disrupts them, eventually causing neurodegeneration (Fox et al., 2011; Liu et al., 2012; Menkes-Caspi et al., 2015). Both tau and Aβ cause synaptic damage in soluble and fibrillar forms, individually and together (Spires-Jones and Hyman, 2014); where and how they interact and whether they enable each other's spread is still widely unknown, although *APOE* allele status and GSK3 activity have, among others, been identified as potential upstream drivers linking together diverging pathways (Small and Duff, 2008). A fundamental unanswered question is whether Aβ deposition facilitates tau spread outside MTL, or whether tau spread outside MTL results in neocortical Aβ deposition.

Tau Is Associated with Cross-sectional and Longitudinal Cognitive Measures in Healthy Aging

Tau and amyloid pathology reportedly also have diverging effects on cognition. Tau, particularly in MTL, is abundant in aging and not exclusive to AD. Concordantly, episodic memory decline is a common feature of normal aging (Deary et al., 2009). Although MTL tau pathology at autopsy has consistently been found more closely associated with cognition than has Aβ (Arriagada et al., 1992; Bennett et al., 2012; Ghoshal et al., 2002; Mitchell et al., 2002; Nelson et al., 2012; Rolstad et al., 2013), the majority of these studies examined individuals with cognitive impairment and dementia. The importance of MTL tau deposition in relation to memory decline seen in normal cognitive aging is unclear. Notably, we found that cross-sectional and longitudinal decline in performance in tests for episodic memory in OA were strongly related to MTL tracer uptake in Braak ROI I/II, seemingly independent of cortical amyloid pathology. Our results strengthen the hypothesis that tau pathology plays a key role in memory decline in aging, which is also strongly related to dysfunction of MTL structures (Tromp et al., 2015). A potential caveat is that cognitive decline can be observed at a stage where only a small number of MTL neurons are affected by tau pathology (Hoover et al., 2010), and soluble and pre-NFT forms of tau impair memory-consolidating hippocampal function; this must be considered when interpreting tau PET data measuring PHF tau. In addition, the results of our regression models were based on a small sample and driven by a few influential data points but were confirmed by nonparametric voxelwise analyses.

We also found decline in global cognition associated with tau in all Braak ROIs, but the effect for cortical regions outside Braak ROIs I–IV was related to the presence of cortical Aβ. These results are in agreement with recent findings across a sample of cognitively normal, mild cognitive impairment (MCI), and AD participants that clinical impairment was associated with tracer retention in inferior temporal cortex, which was also related to mean cortical PIB (Johnson et al., 2016). This suggests that while changes in episodic memory may be caused by age-related MTL tau accumulation, longitudinal changes in global cognition may be induced by synergistic effects of tau and Aβ pathology when both are present outside MTL regions. We also found that global Aβ was related to retrospective longitudinal decline in global cognition, consistent with findings from a series of studies using CSF and PET measures of Aβ in relation to cognitive performance (Fagan et al., 2007; Landau et al., 2012; Villemagne et al., 2013). The effect of Aβ on global cognitive decline, however, only remained statistically significant when Braak ROI I/II, not Braak III-VI ROI data, were added to the respective model, again suggesting that longitudinal cognitive decline in our cohort cannot be explained by Aβ or tau pathology alone.

Conclusions

These findings indicate that PHF-tau deposition can be tracked by AV-1451 PET in living humans with results that confirm and extend information obtained from neuropathological studies. The pattern of tracer retention is qualitatively similar to tau deposition patterns reported in many autopsy studies. In addition, we demonstrate the feasibility of pathological staging of living individuals for tau pathology and demonstrate

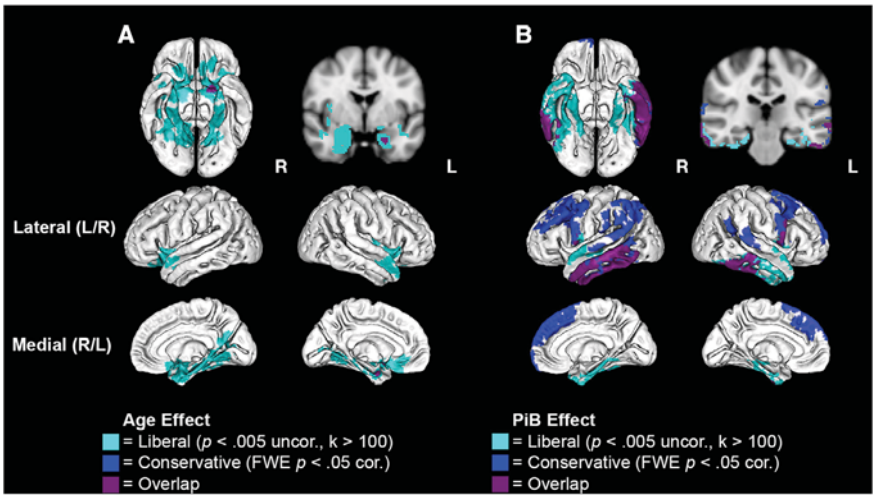

Figure 6. Age, Aβ, and Tau Associations among OA

(A) Positive associations between chronological age and AV-1451 accumulation in OA (n = 33), controlling for global PiB DVR, exist in medial temporal and ventral frontal subregions. Note all Age FWE results (left MTL, ventral frontal) are overlapped and only liberal and overlap colors are visible.

(B) Positive associations between PiB DVR and AV-1451 accumulation, controlling for chronological age, appear in additional temporal regions, as well as in parietal and frontal cortex. All results from voxelwise nonparametric regression, with mean-centered covariates of age (years) and PiB (global cortical DVR). Multiple statistical thresholding approaches were considered: a combined uncorrected cluster (k > 100 voxels) plus height (p < 0.005) threshold ("liberal"), and an FWE p < 0.05 correction ("conservative"). See also Table S4, Figure S4, and Movie S4.

dissociated relationships between age and Aβ that support a model of interaction between these proteins in AD pathogenesis. The relationship between tau and cognition, even in cognitively normal older people, suggests a crucial role for this protein in aging, supporting the use of tau imaging in naturalistic studies and therapeutic trials.

EXPERIMENTAL PROCEDURES

Participants

We recruited 33 cognitively healthy older adults (OA) and five cognitively healthy young adults (YA) from the Berkeley Aging Cohort Study (BACS), an ongoing longitudinal study of cognitive aging. BACS eligibility requirements included no MRI or PET contraindications, living independently in the community, and normal performance on neuropsychological examination (see below and Supplemental Experimental Procedures for details). Furthermore, 15 AD patients were recruited from the UCSF MAC. All AD patients underwent standard dementia screening including medical history and physical examination, caregiver interview, brain MRI, and neuropsychological testing; note the AD sample studied here clinically does not represent a typical group (see Supplemental Experimental Procedures). Clinical diagnosis was established by consensus in a multidisciplinary team; all AD patients fulfilled National Institute on Aging-Alzheimer's Association (NIA-AA) criteria for probable Alzheimer's disease (McKhann et al., 2011). One participant was diagnosed with behavioral/dysexecutive variant of AD, one with early-onset amnestic AD, three with late-onset amnestic AD, four with logopenic variant primary progressive aphasia, and six with posterior cortical atrophy (Ossenkoppele et al., 2015b, 2015c). All participants underwent structural MRI, ^{11}C-PiB, and ^{18}F-AV-1451 PET imaging, and detailed neuropsychological assessment, as described below. The Institutional Review Boards of all participating institutions approved the study and informed consent was obtained from all participants. YA and AD participants were used only in the Braak staging analysis.

PET Acquisition

[^{11}C] Pittsburgh-B (PiB) was synthesized at the Lawrence Berkeley National Laboratory (LBNL) Biomedical Isotope Facility (BIF), using a protocol described in detail previously (Mathis et al., 2003). We conducted PiB PET imaging in 3D acquisition mode using either (OA n = 6) an ECAT EXACT HR scanner or (OA n = 27, AD n = 14) a BIOGRAPH PET/CT Truepoint 6 scanner (Siemens Medical Systems). Criteria for PiB positivity did not differ between PET scanners used for PiB acquisition, and PiB PET DVR values have been shown not to significantly differ between scanners (Elman et al., 2014). Immediately after the intravenous injection of approximately 15 mCi of PiB, 90 min of dynamic acquisition frames were obtained (4 × 15, 8 × 30, 9 × 60, 2 × 180, 10 × 300, and 2 × 600 s). For each PiB scan, a 10 min transmission scan or a CT were obtained for attenuation correction. PiB PET images were reconstructed using an ordered subset expectation maximization algorithm with weighted attenuation and smoothed with a 4 mm Gaussian kernel with scatter correction.

^{18}F-AV-1451 (T807) PET imaging was performed within 0 and 335 days of PiB PET. AV-1451 was also synthesized at the LBNL BIF using a GE TracerLab FXN-Pro synthesis module with a modified protocol based on that supplied by Avid radiopharmaceuticals. AV-1451 PET imaging was conducted on the BIOGRAPH PET/CT scanner. Participants were injected with 10 mCi of tracer and participated in one of two acquisition schemes: full dynamic scans (YA n = 5, OA n = 23, AD n = 11; 0–100 min post injection with 4 × 15, 8 × 30, 9 × 60 s, and 2 × 3, 16 × 5 min frames; and 120–150 min, 6 × 5 min frames), or 75–115 min scans (OA n = 10, AD n = 4; 8 × 5 min frames). A CT scan was performed before the start of each emission acquisition. For all analyses, we used SUVR data collected from 80–100 min, determined to be the best time frame and processing scheme for a range of clinical diagnoses studied using this tracer in separate pharmacokinetic studies (e.g., Chien et al., 2013). AV-1451 PET images were reconstructed using an ordered subset expectation maximization algorithm with weighted attenuation and smoothed with a 4 mm Gaussian kernel with scatter correction.

MRI Acquisition

All cognitively healthy participants (YA and OA) underwent MRI on a 1.5T Siemens Magnetom Avanto scanner at LBNL; this session included a high-resolution T1-weighted magnetization prepared rapid gradient echo (MPRAGE) scan (TR/TE = 2110/3.58 ms, FA = 15°, 1 × 1 × 1 mm resolution). All AD patients underwent MRI at the UCSF Neuroimaging Center on a 3T Siemens Tim Trio scanner; this session included a 1 × 1 × 1 mm resolution T1-weighted MPRAGE that was acquired as described previously (Ossenkoppele et al., 2015a).

PET Image Processing

PiB data were realigned, and frames corresponding to the first 20 min of acquisition were averaged and coregistered to the participant's structural MRI. Distribution volume ratios (DVRs) for PiB images were created using Logan graphical analysis (35–90 min postinjection) and a gray matter masked cerebellum reference region (Logan et al., 1996; Price et al., 2005). DVR voxelwise images were created, and global cortical PiB DVR ("global PiB") values, derived using native space FreeSurfer-derived cortical gray matter masks, were calculated for each participant for use in analyses and classification of PiB positivity (Mormino et al., 2011). Participants were described as PiB positive if their global PiB DVR was at or above a selected threshold of 1.06, and PiB negative otherwise; this threshold is adapted from previous thresholds developed in our laboratory to examine early amyloid positivity in healthy controls (Mormino et al., 2012).

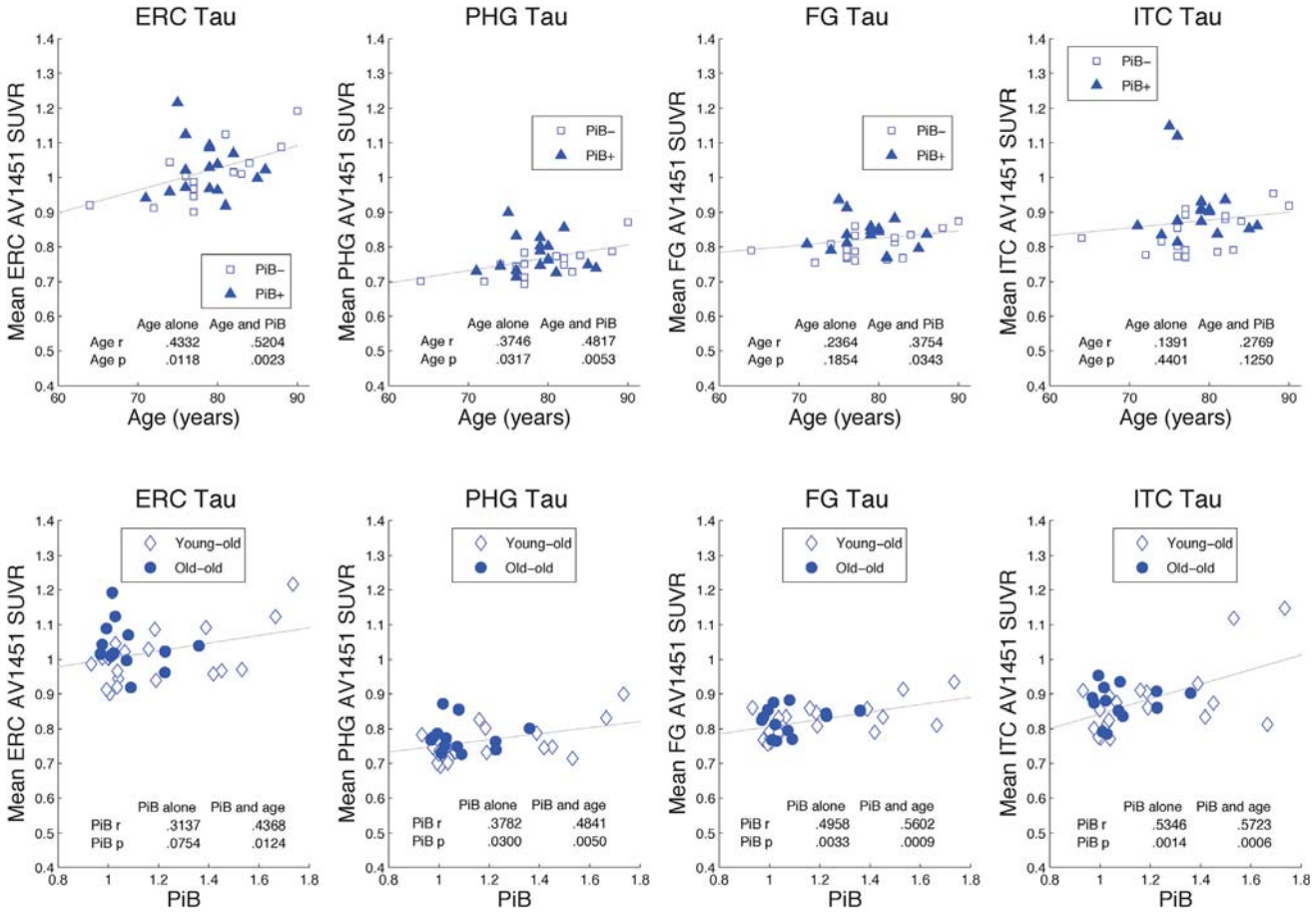

Figure 7. Temporal Lobe Regional Patterns of Tau Accumulation in OA

Relations of bilateral temporal ROI AV-1451 SUVR values with age (top row) and with PiB DVR (bottom row). Left to right within each row represents a medial-to-lateral path across the inferior aspect of temporal cortex. Also shown are regression results for models with one or two independent variables. ROIs: entorhinal cortex, ERC; parahippocampal gyrus, PHG; fusiform gyrus, FG; inferior temporal cortex, ITC. In bottom row, participants are median-split by age for descriptive purposes (young-old: <79 years, old-old: ≥79 years).

For AV-1451 scanning, we recruited equal numbers of OA participants above and below this PiB value. However, no primary hypotheses involved PiB status.

AV-1451 data were realigned, and the mean of all frames was used to coregister AV-1451 data to each participant's MRI. For the separate acquisition schemes, we used separate coregistration approaches. When available, we used 0–150 min data for participants with full dynamic scans and 80–100 data for participants with only 75–115 min scans. Coregistration approach (0–150 versus 80–100 min) did not differentially affect ROI segmentation. We created AV-1451 standardized uptake value (SUV) images based on mean uptake over 80–100 min postinjection normalized to uptake in a gray matter masked cerebellum reference region to create voxelwise SUV ratio (SUVR) images in each participant's MRI native space.

MRI Processing

T1 MPRAGE scans were processed as described previously using FreeSurfer version 5.1 (http://surfer.nmr.mgh.harvard.edu/) (Mormino et al., 2009). FreeSurfer was used to delineate anatomical ROI masks for multiple brain regions on the native space MRI (coregistered to the PET scans); segmentations were manually checked for accuracy. The gray matter cerebellum mask used as a reference region for PiB and AV-1451 PET was derived in this way. MRI images were also segmented into brain tissue types using SPM8 (http://www.fil.ion.ucl.ac.uk/spm) and a global gray matter (GM) volume value was calculated per participant by identifying and summing all brain voxels with gray matter probability >0.5 for use as a covariate of no interest in specific analyses.

In Vivo Braak Staging Data Preprocessing

Following coregistration of AV-1451 PET images to MRI, and parcellation by FreeSurfer, we employed the Geometric Transfer Matrix approach according to Rousset (Rousset et al., 1998) for partial volume correction (PVC) of ROI data (see Figure S1 and Supplemental Experimental Procedures for details). We then created bilateral Braak stage ROIs that anatomically approximated the Braak staging regions of AD-related tau pathology, following descriptions from previous publications (Alafuzoff et al., 2008; Braak et al., 2006, 2011; Braak and Braak, 1991). Braak ROIs were created by combining FreeSurfer ROIs into non-overlapping Braak regions I/II, III/IV, and V/VI. Braak stage ROI composition is listed in Table S1; 3D renderings of the Braak stage ROIs are shown in Movies S1, S2, and S3. Braak stage ROIs I/II corresponded to the transentorhinal stage, III/IV to the limbic stage, and V/VI to the isocortical Braak stage. Braak ROI values were extracted taking ROI-volume-weighted averages of AV-1451 retention in each Braak region.

Voxelwise AV-1451 Data Preprocessing

To examine voxelwise associations of AV-1451 with chronological age, global PiB, and cognition, we warped MRI scans for all OA (n = 33) to the FSL MNI152 2 mm space template (http://www.fmrib.ox.ac.uk/fsl). Normalization was performed using Advanced Normalization Tools (ANTS; http://stnava.github.io/ANTs/) with the use of a study-specific intermediate template created from the 33 BACS OA. Results were similar when using SPM8 for group normalization. After estimating linear and nonlinear transformations from each native

space into MNI152 space, transformations were concatenated and applied to the MRI and coregistered AV-1451 PET images. To allow us to focus on cortical AV-1451 binding patterns (as some off-target binding is known to occur in subcortical regions, see Figure 1), we employed a FreeSurfer segmentation on the MNI152 template structural MRI, and created a mask using all cortical brain regions. To reduce contributions of CSF and noise to the analysis, we filtered out likely CSF voxels at the gray matter/CSF boundary in template space (coefficient of variation [CoV] of AV-1451 data thresholded $\geq$ 0.25). A testing mask (i.e., voxels highly likely to be cortical gray matter) was created from the resulting image. AV-1451 images were then masked and smoothed by a 4 mm FWHM kernel before analysis.

Neuropsychological Examination

Cross-sectional (closest to AV-1451 scan) and retrospective longitudinal (prior to AV-1451 scan) neuropsychological data of the BACS OA were employed in this study. Thirty out of 33 OA had longitudinal data, with 4.0 ± 2.2 testing sessions over a period of 4.1 ± 2.2 years. For each testing session, factor scores were calculated for episodic memory, working memory, and executive function/processing speed domains using a maximum likelihood analysis adjusted for test results from a larger sample of 346 BACS OA participants (see Supplemental Experimental Procedures for details). In addition, a global cognition measure was created as an average of the three factor scores.

To assess change in cognition over time, slopes of change in the respective cognitive domain were generated using a linear mixed effects model (Figure S5). Random effects included inter-individual intercept and time between neuropsychological examinations. No fixed effects were included as potential covariates were included in subsequent analyses.

Statistical Analysis

In Vivo Braak Staging Based on AV-1451 Uptake

To create thresholds allowing assignment of Braak stages to individuals based exclusively on native space AV-1451 PET ROI data, we employed conditional inference tree analysis (Figure S2; using R [v. 3.1.2]; Ihaka and Gentleman, 1996), and the package *party* and its function *ctree*. *Ctree* performs nonparametric binary recursive partitioning using the following steps: (1) test the global null hypothesis of independence between any input variables and the response (which may be multivariate as well), and stop if this hypothesis cannot be rejected. Otherwise select the input variable with strongest association to the response. This association is measured by a p value corresponding to a test for the partial null hypothesis of a single input variable and the response. (2) Implement a binary split in the selected input variable. (3) Recursively repeat steps (1) and (2).

ROI-Based Association of AV-1451 Uptake and Cognitive Measures

Least-squares regression was employed to explore the direct effect of AV-1451 uptake in Braak stage ROIs on cross-sectional and retrospective change in cognitive performance in OA (n = 33). We adjusted models for age and sex to avoid bias; the effect of education was found to be non-significant and thus not modeled. All tests were two-sided, with significance determined at $p < 0.05$; the term "effect" was used as per statistical convention to describe associations between variables. All analyses were done using R (v. 3.2.1). We also examined whether the p value for the association between AV-1451 and cognition changed from significant to non-significant when adjusting for PiB. Furthermore, we explored the reverse relationship, i.e., the direct effect of PiB on cognition and the change in significance of this model when Braak ROI AV-1451 data was added to the model.

Voxelwise Association of AV-1451 Uptake with Cognitive Measures

Template space voxelwise nonparametric regressions (FSL randomise; threshold-free cluster enhancement [TFCE]; 50,000 permutations; cortical mask described above) tested where AV-1451 binding was related to cognitive factor scores and slopes in OA. Voxelwise analyses were conducted with terms of age and sex included in the model. Voxelwise cognitive results are presented with a $p < 0.005$ (uncorrected) height plus 100 voxel cluster extent threshold.

Voxelwise Associations of Age and Global PiB with AV-1451 Uptake

Template space voxelwise nonparametric regressions (FSL randomise; TFCE; 50,000 permutations; cortical mask described above) tested where AV-1451 binding was related to age or PiB in OA (see plot of age versus PiB DVR in Figure S4, and mean AV-1451 images by PiB level in Movie S4). Voxelwise analyses were conducted with terms of chronological age and global PiB DVR in the model. Voxelwise results are presented with both a $p < 0.005$ (uncorrected) height plus 100 voxel cluster extent ("liberal") threshold, and with a $p < 0.05$ (FWE-corrected) height ("conservative") threshold. The use of combined voxel and cluster-extent thresholds, and the use of TFCE, means that conservative threshold results are not exclusively a subset of liberal results; this was done in order to better understand the spatial pattern of AV-1451 results. Finally, ROI analyses on template space AV-1451 data (using FreeSurfer-segmented ROIs in MNI152 template space) used MATLAB to assess relations of age or PiB DVR (linear regression) with bilateral mean ROI AV-1451 signal.

SUPPLEMENTAL INFORMATION

Supplemental Information includes Supplemental Experimental Procedures, five figures, four tables, and four movies and can be found with this article online at http://dx.doi.org/10.1016/j.neuron.2016.01.028.

AUTHOR CONTRIBUTIONS

Conceptualization, M.S., S.N.L., and W.J.J.; Methodology, M.S., S.N.L, D.R.S., and W.J.J.; Formal Analysis, M.S., S.N.L., D.R.S., and S.L.B.; Resources, J.P.O. and M.J.; Investigation, S.L.B., J.W.V., J.F., and H.D.S.; Writing – Original Draft, M.S., S.N.L., and W.J.J.; Writing – Review & Editing, M.S., S.N.L., D.R.S., J.P.O., M.J., R.O., S.L.B., G.D.R., and W.J.J.; Supervision, W.J.J.; Funding Acquisition, G.D.R. and W.J.J.

ACKNOWLEDGMENTS

We thank Philip Insel for statistical analyses support, and Dr. Bruce Miller and the UCSF Alzheimer's Disease Research Center (NIH grant P50-AG23501) for AD patient evaluations and referrals. This research was supported by NIH grants AG034570 (W.J.J.), R01-AG045611 (G.D.R.), and P50-AG23501 (Dr. Bruce L. Miller, G.D.R.), the Swedish Medical Association (M.S.), Tau Consortium (W.J.J., G.D.R.), the Blanceflor Foundation (M.S.), John Douglas French Alzheimer's Foundation (G.D.R.), the Marie Curie FP7 International Outgoing Fellowship (628812) (R.O.), and the donors of (Alzheimer's Disease Research), a program of BrightFocus Foundation (R.O.). Avid Radiopharmaceuticals enabled use of the ^{18}F-AV-1451 tracer but did not provide direct funding and were not involved in data analysis or interpretation. G.D.R. receives research support from Avid Radiopharmaceuticals, which owns the rights to the ^{18}F-AV-1451 compound. W.J.J. has served as a consultant to Bioclinica, Genentech, and Novartis pharmaceuticals.

Received: October 28, 2015
Revised: December 12, 2015
Accepted: January 13, 2016
Published: March 2, 2016

REFERENCES

Alafuzoff, I., Arzberger, T., Al-Sarraj, S., Bodi, I., Bogdanovic, N., Braak, H., Bugiani, O., Del-Tredici, K., Ferrer, I., Gelpi, E., et al. (2008). Staging of neurofibrillary pathology in Alzheimer's disease: a study of the BrainNet Europe Consortium. Brain Pathol. *18*, 484–496.

Arriagada, P.V., Growdon, J.H., Hedley-Whyte, E.T., and Hyman, B.T. (1992). Neurofibrillary tangles but not senile plaques parallel duration and severity of Alzheimer's disease. Neurology *42*, 631–639.

Bennett, D.A., Schneider, J.A., Arvanitakis, Z., Kelly, J.F., Aggarwal, N.T., Shah, R.C., and Wilson, R.S. (2006). Neuropathology of older persons without cognitive impairment from two community-based studies. Neurology *66*, 1837–1844.

Bennett, D.A., Wilson, R.S., Boyle, P.A., Buchman, A.S., and Schneider, J.A. (2012). Relation of neuropathology to cognition in persons without cognitive impairment. Ann. Neurol. *72*, 599–609.

Bouras, C., Hof, P.R., Giannakopoulos, P., Michel, J.P., and Morrison, J.H. (1994). Regional distribution of neurofibrillary tangles and senile plaques in

the cerebral cortex of elderly patients: a quantitative evaluation of a one-year autopsy population from a geriatric hospital. Cereb. Cortex *4*, 138–150.

Braak, H., and Braak, E. (1991). Neuropathological stageing of Alzheimer-related changes. Acta Neuropathol. *82*, 239–259.

Braak, H., and Braak, E. (1997). Frequency of stages of Alzheimer-related lesions in different age categories. Neurobiol. Aging *18*, 351–357.

Braak, H., Braak, E., Bohl, J., and Reintjes, R. (1996). Age, neurofibrillary changes, A beta-amyloid and the onset of Alzheimer's disease. Neurosci. Lett. *210*, 87–90.

Braak, H., Alafuzoff, I., Arzberger, T., Kretzschmar, H., and Del Tredici, K. (2006). Staging of Alzheimer disease-associated neurofibrillary pathology using paraffin sections and immunocytochemistry. Acta Neuropathol. *112*, 389–404.

Braak, H., Thal, D.R., Ghebremedhin, E., and Del Tredici, K. (2011). Stages of the pathologic process in Alzheimer disease: age categories from 1 to 100 years. J. Neuropathol. Exp. Neurol. *70*, 960–969.

Chien, D.T., Bahri, S., Szardenings, A.K., Walsh, J.C., Mu, F., Su, M.-Y., Shankle, W.R., Elizarov, A., and Kolb, H.C. (2013). Early clinical PET imaging results with the novel PHF-tau radioligand [F-18]-T807. J. Alzheimers Dis. *34*, 457–468.

Crary, J.F., Trojanowski, J.Q., Schneider, J.A., Abisambra, J.F., Abner, E.L., Alafuzoff, I., Arnold, S.E., Attems, J., Beach, T.G., Bigio, E.H., et al. (2014). Primary age-related tauopathy (PART): a common pathology associated with human aging. Acta Neuropathol. *128*, 755–766.

Davis, D.G., Schmitt, F.A., Wekstein, D.R., and Markesbery, W.R. (1999). Alzheimer neuropathologic alterations in aged cognitively normal subjects. J. Neuropathol. Exp. Neurol. *58*, 376–388.

Deary, I.J., Corley, J., Gow, A.J., Harris, S.E., Houlihan, L.M., Marioni, R.E., Penke, L., Rafnsson, S.B., and Starr, J.M. (2009). Age-associated cognitive decline. Br. Med. Bull. *92*, 135–152.

Duyckaerts, C., Braak, H., Brion, J.P., Buée, L., Del Tredici, K., Goedert, M., Halliday, G., Neumann, M., Spillantini, M.G., Tolnay, M., and Uchihara, T. (2015). PART is part of Alzheimer disease. Acta Neuropathol. *129*, 749–756.

Elman, J.A., Oh, H., Madison, C.M., Baker, S.L., Vogel, J.W., Marks, S.M., Crowley, S., O'Neil, J.P., and Jagust, W.J. (2014). Neural compensation in older people with brain amyloid-β deposition. Nat. Neurosci. *17*, 1316–1318.

Fagan, A.M., Roe, C.M., Xiong, C., Mintun, M.A., Morris, J.C., and Holtzman, D.M. (2007). Cerebrospinal fluid tau/beta-amyloid(42) ratio as a prediction of cognitive decline in nondemented older adults. Arch. Neurol. *64*, 343–349.

Fornicola, W., Pelcovits, A., Li, B.-X., Heath, J., Perry, G., and Castellani, R.J. (2014). Alzheimer Disease Pathology in Middle Age Reveals a Spatial-Temporal Disconnect Between Amyloid-β and Phosphorylated Tau. Open Neurol. J. *8*, 22–26.

Fox, L.M., William, C.M., Adamowicz, D.H., Pitstick, R., Carlson, G.A., Spires-Jones, T.L., and Hyman, B.T. (2011). Soluble tau species, not neurofibrillary aggregates, disrupt neural system integration in a tau transgenic model. J. Neuropathol. Exp. Neurol. *70*, 588–595.

Ghoshal, N., García-Sierra, F., Wuu, J., Leurgans, S., Bennett, D.A., Berry, R.W., and Binder, L.I. (2002). Tau conformational changes correspond to impairments of episodic memory in mild cognitive impairment and Alzheimer's disease. Exp. Neurol. *177*, 475–493.

Guillozet, A.L., Weintraub, S., Mash, D.C., and Mesulam, M.-M. (2003). Neurofibrillary tangles, amyloid, and memory in aging and mild cognitive impairment. Arch. Neurol. *60*, 729–736.

Hoover, B.R., Reed, M.N., Su, J., Penrod, R.D., Kotilinek, L.A., Grant, M.K., Pitstick, R., Carlson, G.A., Lanier, L.M., Yuan, L.-L., et al. (2010). Tau mislocalization to dendritic spines mediates synaptic dysfunction independently of neurodegeneration. Neuron *68*, 1067–1081.

Hyman, B.T., Phelps, C.H., Beach, T.G., Bigio, E.H., Cairns, N.J., Carrillo, M.C., Dickson, D.W., Duyckaerts, C., Frosch, M.P., Masliah, E., et al. (2012). National Institute on Aging-Alzheimer's Association guidelines for the neuropathologic assessment of Alzheimer's disease. Alzheimers Dement. *8*, 1–13.

Ihaka, R., and Gentleman, R. (1996). R: a laokaynguage for data analysis and graphics. J. Comput. Graph. Stat. *5*, 299–314.

Jack, C.R., Jr., Knopman, D.S., Jagust, W.J., Petersen, R.C., Weiner, M.W., Aisen, P.S., Shaw, L.M., Vemuri, P., Wiste, H.J., Weigand, S.D., et al. (2013). Tracking pathophysiological processes in Alzheimer's disease: an updated hypothetical model of dynamic biomarkers. Lancet Neurol. *12*, 207–216.

Jellinger, K.A., Alafuzoff, I., Attems, J., Beach, T.G., Cairns, N.J., Crary, J.F., Dickson, D.W., Hof, P.R., Hyman, B.T., Jack, C.R., Jr., et al. (2015). PART, a distinct tauopathy, different from classical sporadic Alzheimer disease. Acta Neuropathol. *129*, 757–762.

Johnson, K.A., Schultz, A., Betensky, R.A., Becker, J.A., Sepulcre, J., Rentz, D., Mormino, E., Chhatwal, J., Amariglio, R., Papp, K., et al. (2016). Tau PET imaging in aging and early Alzheimer's disease. Ann. Neurol. *79*, 110–119.

Landau, S.M., Mintun, M.A., Joshi, A.D., Koeppe, R.A., Petersen, R.C., Aisen, P.S., Weiner, M.W., and Jagust, W.J.; Alzheimer's Disease Neuroimaging Initiative (2012). Amyloid deposition, hypometabolism, and longitudinal cognitive decline. Ann. Neurol. *72*, 578–586.

Liu, L., Drouet, V., Wu, J.W., Witter, M.P., Small, S.A., Clelland, C., and Duff, K. (2012). Trans-synaptic spread of tau pathology in vivo. PLoS ONE *7*, e31302.

Logan, J., Fowler, J.S., Volkow, N.D., Wang, G.J., Ding, Y.S., and Alexoff, D.L. (1996). Distribution volume ratios without blood sampling from graphical analysis of PET data. J. Cereb. Blood Flow Metab. *16*, 834–840.

Marquie, M., Normandin, M.D., Vanderburg, C.R., Costantino, I., Bien, E.A., Rycyna, L.G., Klunk, W.E., Mathis, C.A., Ikonomovic, M.D., Debnath, M.L., et al. (2015). Validating novel tau PET tracer [F-18]-AV-1451 (T807) on postmortem brain tissue. Ann. Neurol. *78*, 787–800.

Mathis, C.A., Wang, Y., Holt, D.P., Huang, G.F., Debnath, M.L., and Klunk, W.E. (2003). Synthesis and evaluation of 11C-labeled 6-substituted 2-arylbenzothiazoles as amyloid imaging agents. J. Med. Chem. *46*, 2740–2754.

McKhann, G.M., Knopman, D.S., Chertkow, H., Hyman, B.T., Jack, C.R., Jr., Kawas, C.H., Klunk, W.E., Koroshetz, W.J., Manly, J.J., Mayeux, R., et al. (2011). The diagnosis of dementia due to Alzheimer's disease: recommendations from the National Institute on Aging-Alzheimer's Association workgroups on diagnostic guidelines for Alzheimer's disease. Alzheimers Dement. *7*, 263–269.

Menkes-Caspi, N., Yamin, H.G., Kellner, V., Spires-Jones, T.L., Cohen, D., and Stern, E.A. (2015). Pathological tau disrupts ongoing network activity. Neuron *85*, 959–966.

Mitchell, T.W., Mufson, E.J., Schneider, J.A., Cochran, E.J., Nissanov, J., Han, L.-Y., Bienias, J.L., Lee, V.M.Y., Trojanowski, J.Q., Bennett, D.A., and Arnold, S.E. (2002). Parahippocampal tau pathology in healthy aging, mild cognitive impairment, and early Alzheimer's disease. Ann. Neurol. *51*, 182–189.

Mormino, E.C., Kluth, J.T., Madison, C.M., Rabinovici, G.D., Baker, S.L., Miller, B.L., Koeppe, R.A., Mathis, C.A., Weiner, M.W., and Jagust, W.J.; Alzheimer's Disease Neuroimaging Initiative (2009). Episodic memory loss is related to hippocampal-mediated beta-amyloid deposition in elderly subjects. Brain *132*, 1310–1323.

Mormino, E.C., Smiljic, A., Hayenga, A.O., Onami, S.H., Greicius, M.D., Rabinovici, G.D., Janabi, M., Baker, S.L., Yen, I.V., Madison, C.M., et al. (2011). Relationships between β-amyloid and functional connectivity in different components of the default mode network in aging. Cereb. Cortex *21*, 2399–2407.

Mormino, E.C., Brandel, M.G., Madison, C.M., Rabinovici, G.D., Marks, S., Baker, S.L., and Jagust, W.J. (2012). Not quite PIB-positive, not quite PIB-negative: slight PIB elevations in elderly normal control subjects are biologically relevant. Neuroimage *59*, 1152–1160.

Murray, M.E., Graff-Radford, N.R., Ross, O.A., Petersen, R.C., Duara, R., and Dickson, D.W. (2011). Neuropathologically defined subtypes of Alzheimer's disease with distinct clinical characteristics: a retrospective study. Lancet Neurol. *10*, 785–796.

Nelson, P.T., Alafuzoff, I., Bigio, E.H., Bouras, C., Braak, H., Cairns, N.J., Castellani, R.J., Crain, B.J., Davies, P., Del Tredici, K., et al. (2012). Correlation

of Alzheimer disease neuropathologic changes with cognitive status: a review of the literature. J. Neuropathol. Exp. Neurol. *71*, 362–381.

Ossenkoppele, R., Cohn-Sheehy, B.I., La Joie, R., Vogel, J.W., Möller, C., Lehmann, M., van Berckel, B.N.M., Seeley, W.W., Pijnenburg, Y.A., Gorno-Tempini, M.L., et al. (2015a). Atrophy patterns in early clinical stages across distinct phenotypes of Alzheimer's disease. Hum. Brain Mapp. *36*, 4421–4437.

Ossenkoppele, R., Pijnenburg, Y.A.L., Perry, D.C., Cohn-Sheehy, B.I., Scheltens, N.M.E., Vogel, J.W., Kramer, J.H., van der Vlies, A.E., Joie, R.L., Rosen, H.J., et al. (2015b). The behavioural/dysexecutive variant of Alzheimer's disease: clinical, neuroimaging and pathological features. Brain *138*, 2732–2749.

Ossenkoppele, R., Schonhaut, D.R., Baker, S.L., O'Neil, J.P., Janabi, M., Ghosh, P.M., Santos, M., Miller, Z.A., Bettcher, B.M., Gorno-Tempini, M.L., et al. (2015c). Tau, amyloid, and hypometabolism in a patient with posterior cortical atrophy. Ann. Neurol. *77*, 338–342.

Price, J.L., and Morris, J.C. (1999). Tangles and plaques in nondemented aging and "preclinical" Alzheimer's disease. Ann. Neurol. *45*, 358–368.

Price, J.C., Klunk, W.E., Lopresti, B.J., Lu, X., Hoge, J.A., Ziolko, S.K., Holt, D.P., Meltzer, C.C., DeKosky, S.T., and Mathis, C.A. (2005). Kinetic modeling of amyloid binding in humans using PET imaging and Pittsburgh Compound-B. J. Cereb. Blood Flow Metab. *25*, 1528–1547.

Rolstad, S., Berg, A.I., Bjerke, M., Johansson, B., Zetterberg, H., and Wallin, A. (2013). Cerebrospinal fluid biomarkers mirror rate of cognitive decline. J. Alzheimers Dis. *34*, 949–956.

Rousset, O.G., Ma, Y., and Evans, A.C. (1998). Correction for partial volume effects in PET: principle and validation. J. Nucl. Med. *39*, 904–911.

Serrano-Pozo, A., Frosch, M.P., Masliah, E., and Hyman, B.T. (2011). Neuropathological alterations in Alzheimer disease. Cold Spring Harb. Perspect. Med. *1*, a006189.

Sjögren, M., Vanderstichele, H., Agren, H., Zachrisson, O., Edsbagge, M., Wikkelsø, C., Skoog, I., Wallin, A., Wahlund, L.-O., Marcusson, J., et al. (2001). Tau and Abeta42 in cerebrospinal fluid from healthy adults 21-93 years of age: establishment of reference values. Clin. Chem. *47*, 1776–1781.

Small, S.A., and Duff, K. (2008). Linking Abeta and tau in late-onset Alzheimer's disease: a dual pathway hypothesis. Neuron *60*, 534–542.

Spires-Jones, T.L., and Hyman, B.T. (2014). The intersection of amyloid beta and tau at synapses in Alzheimer's disease. Neuron *82*, 756–771.

Tomlinson, B.E., Blessed, G., and Roth, M. (1968). Observations on the brains of non-demented old people. J. Neurol. Sci. *7*, 331–356.

Tong, J., Meyer, J.H., Furukawa, Y., Boileau, I., Chang, L.-J., Wilson, A.A., Houle, S., and Kish, S.J. (2013). Distribution of monoamine oxidase proteins in human brain: implications for brain imaging studies. J. Cereb. Blood Flow Metab. *33*, 863–871.

Tromp, D., Dufour, A., Lithfous, S., Pebayle, T., and Després, O. (2015). Episodic memory in normal aging and Alzheimer disease: Insights from imaging and behavioral studies. Ageing Res. Rev. *24* (Pt B), 232–262.

van Rossum, I.A., Visser, P.J., Knol, D.L., van der Flier, W.M., Teunissen, C.E., Barkhof, F., Blankenstein, M.A., and Scheltens, P. (2012). Injury markers but not amyloid markers are associated with rapid progression from mild cognitive impairment to dementia in Alzheimer's disease. J. Alzheimers Dis. *29*, 319–327.

Villemagne, V.L., Burnham, S., Bourgeat, P., Brown, B., Ellis, K.A., Salvado, O., Szoeke, C., Macaulay, S.L., Martins, R., Maruff, P., et al.; Australian Imaging Biomarkers and Lifestyle (AIBL) Research Group (2013). Amyloid β deposition, neurodegeneration, and cognitive decline in sporadic Alzheimer's disease: a prospective cohort study. Lancet Neurol. *12*, 357–367.

Xia, C.-F., Arteaga, J., Chen, G., Gangadharmath, U., Gomez, L.F., Kasi, D., Lam, C., Liang, Q., Liu, C., Mocharla, V.P., et al. (2013). [(18)F]T807, a novel tau positron emission tomography imaging agent for Alzheimer's disease. Alzheimers Dement. *9*, 666–676.